Research Article | Vol. 32, No. 16 / 29 Jul 2024 / Optics Express 28090
Optics EXPRESS

Bayesian multi-exposure image fusion for robust high dynamic range ptychography

SHANTANU KODGIRWAR,[1,*] LARS LOETGERING,[2] CHANG LIU,[3,4,5] ALEENA JOSEPH,[5] LEONA LICHT,[3,4,5] DANIEL S. PENAGOS MOLINA,[3,4,5] WILHELM ESCHEN,[3,4,5] JAN ROTHHARDT,[3,4,5,6] AND MICHAEL HABECK[1,7,8]

[1]*Faculty of Medicine, Friedrich Schiller University Jena, 07743 Jena, Germany*
[2]*ZEISS Research Microscopy Solutions, Carl-Zeiss-Promenade 10, 07745 Jena, Germany*
[3]*Helmholtz-Institute Jena, Froebelstieg 3, 07743 Jena, Germany*
[4]*GSI Helmholtzzentrum für Schwerionenforschung, Planckstraße 1, 64291 Darmstadt, Germany*
[5]*Institute of Applied Physics and Abbe Center of Photonics, Friedrich Schiller University Jena, Albert-Einstein-Str. 15, 07745 Jena, Germany*
[6]*Fraunhofer Institute for Applied Optics and Precision Engineering, Albert-Einstein-Str. 7, 07745 Jena, Germany*
[7]*Faculty of Mathematics and Computer Science, Friedrich Schiller University Jena, Ernst-Abbe-Platz 2, 07743 Jena, Germany*
[8]*Max Plank Institute for Multidisciplinary Sciences, Am Fassberg 11, 37077 Goettingen, Germany*
[*]*shantanu.kodgirwar@uni-jena.de*

Abstract: The limited dynamic range of the detector can impede coherent diffractive imaging (CDI) schemes from achieving diffraction-limited resolution. To overcome this limitation, a straightforward approach is to utilize high dynamic range (HDR) imaging through multi-exposure image fusion (MEF). This method involves capturing measurements at different exposure times, spanning from under to overexposure and fusing them into a single HDR image. The conventional MEF technique in ptychography typically involves subtracting the background noise, ignoring the saturated pixels and then merging the acquisitions. However, this approach is inadequate under conditions of low signal-to-noise ratio (SNR). Additionally, variations in illumination intensity significantly affect the phase retrieval process. To address these issues, we propose a Bayesian MEF modeling approach based on a modified Poisson distribution that takes the background and saturation into account. The expectation-maximization (EM) algorithm is employed to infer the model parameters. As demonstrated with synthetic and experimental data, our approach outperforms the conventional MEF method, offering superior phase retrieval under challenging experimental conditions. This work underscores the significance of robust multi-exposure image fusion for ptychography, particularly in imaging shot-noise-dominated weakly scattering specimens or in cases where access to HDR detectors with high SNR is limited. Furthermore, the applicability of the Bayesian MEF approach extends beyond CDI to any imaging scheme that requires HDR treatment. Given this versatility, we provide the implementation of our algorithm as a Python package.

1. Introduction

Ptychography [1,2], a scanning coherent diffractive imaging (CDI) method, has gained popularity as a "lensless" computational imaging scheme allowing for simultaneous phase microscopy and wavefront sensing. This is especially advantageous in the short-wavelength regime [3,4], where the availability of high-quality imaging optics is scarce. This technique involves laterally

#524284 https://doi.org/10.1364/OE.524284
Journal © 2024 Received 20 Mar 2024; revised 10 May 2024; accepted 17 May 2024; published 19 Jul 2024

Optics EXPRESS

moving a thin specimen across localized illumination while recording a series of diffraction patterns. By leveraging the overlap between adjacent scan positions, the captured diffraction data can be transformed into complex-valued reconstructions of the specimen and illumination wavefront using a phase-retrieval algorithm (Fig. 1(a)). The camera exposure time is a critical parameter for the acquisition of diffraction patterns. Photons diffracted towards large angles tend to exhibit lower intensities, resulting in a poorer signal-to-noise ratio (SNR). These photons carry high-spatial-frequency information and are usually accessible through measurements with longer acquisition times. However, this may result in the saturation of the pixels at the center of the diffraction patterns due to the limited dynamic range of the detector. To overcome this limitation, high dynamic range (HDR) imaging can be employed as a preprocessing step in CDI before phase retrieval.

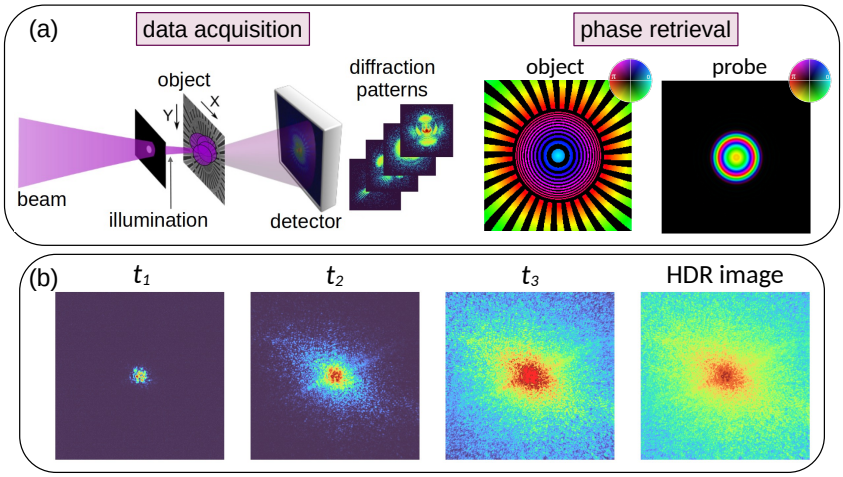

Fig. 1. (a) Principle of conventional ptychography from data acquisition to phase retrieval. (b) Diffraction patterns are recorded at increasing exposure times (bright red pixels are saturated) and fused to achieve a high dynamic range (HDR) image.

Multi-exposure image fusion (MEF) involves recording multiple acquisitions at varying exposure times and fusing them into a single HDR image. Many MEF algorithms have been proposed in the field of computer vision [5–7], with some adoption in microscopy [8–10]. However, to the best of our knowledge, these algorithms have not been directly applied to CDI, primarily because they were not designed for reciprocal space data undergoing phase retrieval. Therefore, in CDI, a predominantly simplistic approach for HDR image fusion has been employed [11–13], referred to here as the *conventional MEF* method. In ptychography, multiple diffraction patterns per scan position are recorded with increasing exposure times and are merged together (see Fig. 1(b)). The conventional MEF method is, however, inadequate in low signal-to-noise ratio (SNR) conditions. For example, diffraction patterns captured from weakly scattering specimens exhibit high levels of shot noise towards large scattering angles. This is due to the diffraction signal being dominated by ballistic (or unscattered) photons. Therefore, performing ptychographic phase retrieval for these specimens is challenging in general [14]. Usually, to overcome this and relax the dynamic range requirements, highly focused structured beams are utilized [15–17]. However, in extreme wavelengths such as the X-ray regime, acquiring high-NA focusing optics is difficult [18,19], thereby lowering the efficacy of these wavefront modulation techniques. Moreover, specialized structuring elements must be added to the beam path [20]. Therefore, MEF algorithms are instrumental in achieving HDR and maintaining high flexibility with regard to the design of the imaging experiments.

Optics EXPRESS

We briefly review the conventional MEF strategy and its limitations before presenting our solution. For every scan position, multiple diffraction patterns $n_i(\boldsymbol{q})$ are recorded for varying acquisition times t_i ($i = 1, \ldots, K$), where K denotes the number of acquisitions and $\boldsymbol{q}$ represents the pixel index. The background estimate $b_i(\boldsymbol{q})$ characterizes camera readout noise. A simple correction for background noise is the subtraction from the diffraction patterns $n_i^+(\boldsymbol{q}) := \max(0, n_i(\boldsymbol{q}) - b_i(\boldsymbol{q}))$, where the max operation enforces nonnegativity. For every acquisition time t_i, there is an associated flux factor $c_i \approx t_i$. These patterns are then fused together into an estimated diffraction intensity $\mathcal{I}(\boldsymbol{q})$ based on maximum likelihood estimation (MLE) under the assumption of Poisson noise (see Supplement 1 section 2):

$$\mathcal{I}(\boldsymbol{q}) = \frac{\sum_i w_i(\boldsymbol{q}) n_i^+(\boldsymbol{q})}{\sum_i w_i(\boldsymbol{q}) c_i(\boldsymbol{q})}, \quad w_i(\boldsymbol{q}) = \begin{cases} 1, & \boldsymbol{q} \text{ is not saturated} \\ 0, & \boldsymbol{q} \text{ is saturated} \end{cases} \tag{1}$$

Pixel-wise binary weight $w_i(\boldsymbol{q})$ ensures that only unsaturated data are used for the fusion process. Even if the exposure time is accurately known, naive MLE estimation suffers from several shortcomings, especially under low-SNR conditions. The background subtraction procedure clips negative values to zero, resulting in a loss of information. The max operation also introduces nonlinearity into intensity estimation, leading to a potential bias [21]. Additionally, this approach ignores saturated data, contributing to another source of information loss and leading to a suboptimal fusion result. Moreover, the flux factors c_i may not be known accurately. In the case of probe intensity fluctuations [22] or if the detector behaves nonlinearly under varying exposure times [23], the conventional approach relies on a heuristic estimate of the flux factors, which affects the quality of fusion. In addition, recognizing the advantage of flexibly modifying the optical intensity, especially by increasing it while adjusting the camera exposure times, can prove beneficial for faster data acquisition. In this case, the uncertainty in c_i will increase, introducing systematic errors in the fused data, thereby significantly affecting phase retrieval.

To tackle these issues and achieve robust HDR imaging in ptychography, we propose a principled Bayesian modeling approach to multi-exposure image fusion which we refer to here as the *Bayesian MEF* method. We start by explaining our probabilistic model, followed by the inference procedure via the expectation-maximization (EM) [24] algorithm. We then demonstrate the efficacy of our approach on synthetic data under low SNR conditions, assuming fixed and accurately known flux factors. Subsequently, we show results from the experimental data in a high SNR, and high photon count setting, where the flux factors are only heuristically known.

2. Bayesian MEF

At the core of a Bayesian approach is the likelihood, a probabilistic model for the data. Here, the model must account for two effects: (a) background noise and (b) saturation owing to overexposure. Suppose we ignore the background noise and saturation effects. In that case, an appropriate likelihood for the i-th exposure is a Poisson distribution with mean $c_i\mathcal{I}(\boldsymbol{q})$, i.e. $n_i(\boldsymbol{q}) \sim \text{Poi}(c_i\mathcal{I}(\boldsymbol{q}))$ where $\sim$ denotes "follows the distribution" [25]. The second component of the Bayesian model is the prior. We assume a Gamma distribution as a prior with shape and scale parameters $\alpha_\mathcal{I}$ and $\beta_\mathcal{I}$. This choice encodes the assumption that $\mathcal{I}$ is non-negative and constant on average, $\mathcal{I}(\boldsymbol{q}) \approx \alpha_\mathcal{I}/\beta_\mathcal{I}$, and the fluctuations in $\mathcal{I}$ are on the order of $\alpha_\mathcal{I}/\beta_\mathcal{I}^2$ [26]. The expectation for a uniform Gamma prior of $\mathcal{I}(\boldsymbol{q})$ can be given as $\alpha_\mathcal{I}/\beta_\mathcal{I} = 1$. To achieve this, we simply provide the same value for $\alpha_\mathcal{I}$ and $\beta_\mathcal{I}$. Here, we choose both of these values to be 10^{-3}, which also avoids instability in the division. In case we have more detailed prior knowledge about $\mathcal{I}$, it can be incorporated by letting $\alpha_\mathcal{I}$ and $\beta_\mathcal{I}$ depend on pixel location $\boldsymbol{q}$. We also assume gamma priors for the unknown flux factors c_i where the hyperparameters α_i, β_i are typically chosen such that the expected flux factor equals the acquisition time $\alpha_i/\beta_i = t_i$. For the special case of $\alpha_i = 1$ which is the exponential distribution, $\beta_i = t_i^{-1}$. The conditional

Optics EXPRESS

posterior distributions for $\mathcal{I}(\boldsymbol{q})$ and c_i are also gamma distributions. The model parameters can be estimated by iterating over the updates

$$\begin{aligned} c_i^{(k+1)} &= \frac{\alpha_i + \sum_{\boldsymbol{q}} n_i(\boldsymbol{q})}{\beta_i + \sum_{\boldsymbol{q}} \mathcal{I}^{(k)}(\boldsymbol{q})}, \\ \mathcal{I}^{(k+1)}(\boldsymbol{q}) &= \frac{\alpha_{\mathcal{I}} + \sum_i n_i(\boldsymbol{q})}{\beta_{\mathcal{I}} + \sum_i c_i^{(k+1)}} \end{aligned} \tag{2}$$

with iteration index denoted by superscript (k). The derivation of the updates in Eq. (2) are provided in Supplement 1 section 3A. For $\alpha_{\mathcal{I}} = \beta_{\mathcal{I}} = 0$, the estimate for $\mathcal{I}(\boldsymbol{q})$ matches the maximum-likelihood estimate for the unsaturated pixels in Eq. (1).

To model the readout noise, we consider the mean $c_i\mathcal{I}(\boldsymbol{q})$ to be shifted by the background mean $b_i(\boldsymbol{q})$ such that $n_i(\boldsymbol{q}) \sim \text{Poi}\,(c_i\mathcal{I}(\boldsymbol{q}) + b_i(\boldsymbol{q}))$. Since the sum of two Poisson distributions is again a Poisson distribution with both means added together, the data can be interpreted as the sum of the background counts generated from $\text{Poi}\,(b_i(\boldsymbol{q}))$ and noisefree counts $n_{\mathcal{I}i}(\boldsymbol{q}) \sim \text{Poi}\,(c_i\mathcal{I}(\boldsymbol{q}))$. Only the sum of the background and noisefree counts is observed; however, $n_{\mathcal{I}i}(\boldsymbol{q})$ can be estimated from $n_i(\boldsymbol{q})$. The conditional posterior of the noisefree counts is a binomial distribution (see Supplement 1 section 3B), and their expected values are

$$\mathbb{E}[n_{\mathcal{I}i}(\boldsymbol{q}) \mid \mathcal{I}(\boldsymbol{q}), c_i, b_i(\boldsymbol{q})] = \frac{c_i\mathcal{I}(\boldsymbol{q})}{c_i\mathcal{I}(\boldsymbol{q}) + b_i(\boldsymbol{q})} n_i(\boldsymbol{q})\,. \tag{3}$$

These are fractions of the observed counts $n_i(\boldsymbol{q})$, which differ from estimating $n_{\mathcal{I}i}(\boldsymbol{q})$ (or $n_i^+(\boldsymbol{q})$ defined earlier) that involves the harsh background subtraction procedure.

To take the saturated pixels into account, we assume that the data $n_i(\boldsymbol{q})$ are *censored* at the detector threshold n^* meaning that they are clipped at a maximum value of n^*. The likelihood is a *(right-) censored* Poisson distribution (i.e., the right tail of the Poisson distribution is not observed). Let $\nu_i(\boldsymbol{q})$ denote the latent uncensored counts, $\nu_i(\boldsymbol{q}) \sim \text{Poi}\,(c_i\mathcal{I}(\boldsymbol{q}) + b_i(\boldsymbol{q}))$, then the observed data can be modeled as $n_i(\boldsymbol{q}) = \nu_i(\boldsymbol{q})$ if $\nu_i(\boldsymbol{q}) < n^*$ (or equivalently, $w_i(\boldsymbol{q}) = 1$), and $n_i(\boldsymbol{q}) = n^*$ if $\nu_i(\boldsymbol{q}) \geq n^*$ (or $w_i(\boldsymbol{q}) = 0$). If we know $\nu_i(\boldsymbol{q})$, then parameter estimation would simplify to background removal under the Poisson model, as in Eq. (3). However, since we do not observe the uncensored counts directly, we have to estimate them. This can be achieved with the following conditional posterior distributions

$$\begin{aligned} \nu_i(\boldsymbol{q}) &\sim \begin{cases} \text{TruncPoi}\,(c_i\mathcal{I}(\boldsymbol{q}) + b_i(\boldsymbol{q}), n^* - 1), & w_i(\boldsymbol{q}) = 0 \\ \text{Poi}\,(c_i\mathcal{I}(\boldsymbol{q}) + b_i(\boldsymbol{q})), & w_i(\boldsymbol{q}) = 1 \end{cases} \\ \nu_{\mathcal{I}i}(\boldsymbol{q}) &\sim \text{Binomial}\left(\nu_i(\boldsymbol{q}), \frac{c_i\mathcal{I}(\boldsymbol{q})}{c_i\mathcal{I}(\boldsymbol{q}) + b_i(\boldsymbol{q})}\right) \\ c_i &\sim \text{Gamma}\,(\alpha_i + \sum_{\boldsymbol{q}} \nu_{\mathcal{I}i}(\boldsymbol{q}), \beta_i + \sum_{\boldsymbol{q}} \mathcal{I}(\boldsymbol{q})) \\ \mathcal{I}(\boldsymbol{q}) &\sim \text{Gamma}\,(\alpha_{\mathcal{I}} + \sum_i \nu_{\mathcal{I}i}(\boldsymbol{q}), \beta_{\mathcal{I}} + \sum_i c_i) \end{aligned} \tag{4}$$

where $\nu_{\mathcal{I}i}(\boldsymbol{q})$ are the noisefree contributions to the uncensored counts $\nu_i(\boldsymbol{q})$ and TruncPoi denotes the truncated Poisson distribution [27]. The model parameters are inferred via the expectation-maximization (EM) algorithm, which is an iterative procedure for MLE or maximum a posteriori (MAP) estimation in the presence of incomplete data. The E-step gives the expectation of the latent counts ν_i, allowing us to estimate the latent noisefree counts $\nu_{\mathcal{I}i}$. In the M-step, the estimate of our model parameters; the fused pattern $\mathcal{I}$ and flux factors c_i are maximized (see Supplement 1 section 3C for details).

Optics EXPRESS

Our EM algorithm, referred to here as Bayesian MEF is summarized in algorithm 1. The key steps are: Estimation of the uncensored counts ν_i via their expected values under the truncated Poisson distribution (line 4), background removal (line 5) analogous to Eq. (3), updating the flux factors (line 6) and estimation of the fused pattern (line 7) analogous to Eq. (2). This procedure iteratively estimates the saturated pixels, reduces the measured background noise, allows the correction of flux factors and fuses the acquisitions for HDR imaging. The implementation of this algorithm can be found as a python package in Ref. [28].

Algorithm 1. Bayesian MEF

1: Initialize $\alpha_{\mathcal{I}} = \beta_{\mathcal{I}} = 0.001$, $\alpha_i = 1.0$ and $\beta_i = t_i^{-1}$ ▷ Initialize hyperparameters

2: Initialize $c_i^{(0)} = t_i$, and $\mathcal{I}^{(0)} = \dfrac{\alpha_{\mathcal{I}} + \sum_i w_i n_i}{\beta_{\mathcal{I}} + \sum_i w_i t_i}$ ▷ Initialize model parameters

3: **repeat**

4: $\quad \nu_i^{(k+1)} \leftarrow w_i n_i + (1 - w_i)\, \mathbb{E}[\nu_i | c_i^{(k)} \mathcal{I}^{(k)} + b_i, n^* - 1]$ ▷ Latent counts

5: $\quad \nu_{\mathcal{I}i}^{(k+1)} \leftarrow \dfrac{c_i^{(k)} \mathcal{I}^{(k)}}{c_i^{(k)} \mathcal{I}^{(k)} + b_i} \nu_i^{(k+1)}$ ▷ Latent noisefree counts

6: $\quad c_i^{(k+1)} \leftarrow \dfrac{\alpha_i + \sum_{\boldsymbol{q}} \nu_{\mathcal{I}i}^{(k+1)}(\boldsymbol{q})}{\beta_i + \sum_{\boldsymbol{q}} \mathcal{I}^{(k)}(\boldsymbol{q})}$ ▷ Flux factors

7: $\quad \mathcal{I}^{(k+1)} \leftarrow \dfrac{\alpha_{\mathcal{I}} + \sum_i \nu_{\mathcal{I}i}^{(k+1)}}{\beta_{\mathcal{I}} + \sum_i c_i^{(k+1)}}$ ▷ Fused image

8: $\quad k \leftarrow k + 1$

9: **until** converge

3. Low SNR synthetic data with known flux factors

To study the performance of Bayesian MEF, we considered synthetic data in a low-SNR setting. We fixed the flux factors $c_i = t_i$ and did not estimate them. To simulate a low-SNR condition, we considered a weakly scattering specimen. Supplement 1 section 4 derives the SNR condition under weak phase object approximation (WPOA) [29]. In general, a phase object is given by $O(\boldsymbol{q}) = \exp\left(i\phi(\boldsymbol{q})\right)$ where $\rho \approx \max\left(\phi(\boldsymbol{q})\right)$ denotes the maximum phase. Smaller values of ρ result in weaker scattering, corresponding to a weakly phase-modulating specimen. To systematically study the impact on ptychographic reconstructions, we simulated the data by varying ρ from weakly scattering $\rho = 0.3$ to strongly scattering $\rho = 1.0$. For a given ρ, the diffraction patterns are simulated using our forward model $n_i(\boldsymbol{q}) \sim \text{Poi}\left(c_i \mathcal{I}(\boldsymbol{q}) + b_i(\boldsymbol{q})\right)$ where the additive background is drawn from the Gaussian distribution $b_i(\boldsymbol{q}) \sim \mathcal{N}(\mu_b, \sigma_b^2)$ [21]. As the dark frames are measured and not estimated, mean background counts μ_b and variance σ_b^2 can be any arbitrary value and does not alter the estimation procedure of the noisefree counts $\nu_{\mathcal{I}i}$ (step 5 in algorithm 1). Usually, the background counts are a small fraction of the actual data and remain fairly constant with low spatial variance. Therefore, we choose $\mu_b = 100$ and $\sigma_b^2 = 0.8$. We set flux-factors c_i to 1, 8, and 64, corresponding to maximum photon counts of $2^7, 2^{10}$ and 2^{13}, respectively. The data was censored at a threshold of 2^{11} causing saturation mainly in the third acquisition. The simulated diffraction patterns are shown in Fig. 2(a), where acquisitions for a specific scan position were generated for $\rho = 1.0$ and $\rho = 0.3$. For the third acquisition ($c_3 = 64$), the number of saturated pixels was ≈ 2.3 times higher for $\rho = 0.3$ than for $\rho = 1.0$, further increasing the level of uncertainty in the fusion of data from the weakly scattering specimen. For each exposure time, we repeated the measurement six times, fusing 18 measurements per scan

Optics EXPRESS

point. While it is not essential to repeat measurements, the proposed Bayesian MEF approach is expected to yield a statistically better estimate of the latent uncensored counts ν_i, particularly in low SNR scenarios. Utilizing fused data from all scan positions, we employed the momentum acceleration (mPIE) [30] phase retrieval algorithm implemented in the open-source package *PtyLab* [31]. Figure 2(b) compares the impact of the MEF methods on the reconstruction of a spokes target as our phase object. The reconstruction quality was significantly better with the Bayesian MEF method for strongly as well as weakly scattering data.

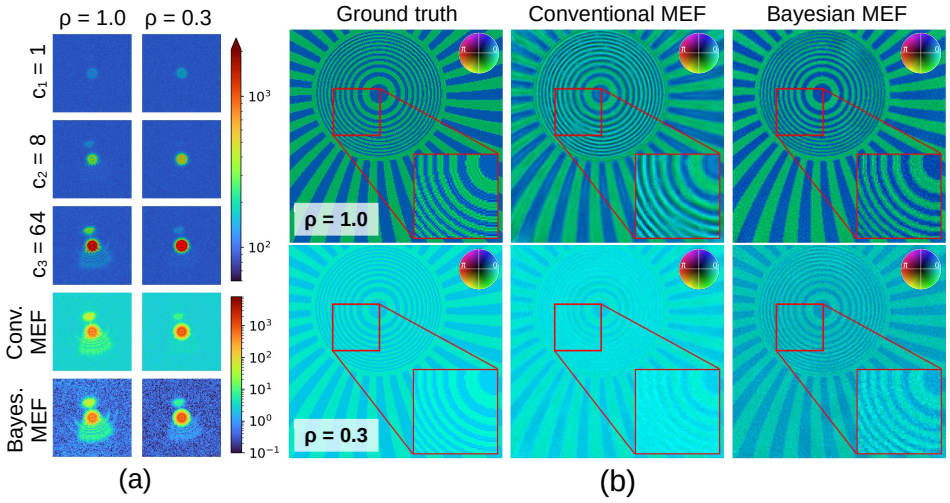

Fig. 2. (a) Synthetic diffraction patterns (log-scale) for a particular scan position under strong scattering ($\rho = 1.0$) and weak scattering ($\rho = 0.3$) corresponding to different flux factors c_i. The third acquisition ($c_3 = 64.0$) exhibits saturation (bright red pixels). The data is then fused with conventional and Bayesian MEF methods. (b) Comparing ptychographic reconstructions (amplitude and phase) of the ground truth with MEF fused result from the synthetic data for $\rho = 1.0$ (top-row) and $\rho = 0.3$ (bottom-row).

To corroborate these results quantitatively, we employed the structural similarity (SSIM) index [32] as our metric. It is defined between windows (spatial patches of the same size) $\mathbf{x}$ from a reference image $\mathbf{X}$ and $\mathbf{y}$ from a test image $\mathbf{Y}$ as

$$\mathrm{SSIM}(\mathbf{x}, \mathbf{y}) = \frac{(2\mu_x\mu_y + C_1)(2\sigma_{xy} + C_2)}{(\mu_x^2 + \mu_y^2 + C_1)(\sigma_x^2 + \sigma_y^2 + C_2)} \tag{5}$$

This provides an estimate of local statistics within the window. In this study, we use a 9×9 window with a circular symmetric Gaussian weighting function $\mathbf{w} = \{w_i | i = 1, 2, \ldots, N\}$ with a standard deviation of 1.0, normalized to the unit sum ($\sum_{i=1}^{N} w_i = 1$). Therefore, the estimates of μ_x and σ_x^2 are given as the weighted mean and variance, respectively.

$$\mu_x = \sum_{i=1}^{N} w_i x_i\,, \quad \sigma_x^2 = \sum_{i=1}^{N} w_i (x_i - \mu_x)^2 \tag{6}$$

This is similar for μ_y and σ_y^2. The weighted covariance σ_{xy} is given as

$$\sigma_{xy} = \sum_{i=1}^{N} w_i (x_i - \mu_x)(y_i - \mu_y) \tag{7}$$

The constants $C_1 = (K_1 L)^2$ and $C_2 = (K_2 L)^2$ prevent instability when either $(\mu_x^2 + \mu_y^2)$ or $(\sigma_x^2 + \sigma_y^2)$ approaches zero. L is the dynamic range that a pixel value can take, which is set to be

Optics EXPRESS

the difference between the maximum and minimum values from our reference and test image $L = \max(\mathbf{X}, \mathbf{Y}) - \min(\mathbf{X}, \mathbf{Y})$. According to the recommendation in Ref. [32], we set the values of $K_1 = 0.01$ and $K_2 = 0.03$. Although these values are somewhat arbitrary, their variations are insensitive to the performance of the SSIM index. If there are M windows that cover the entire image $\mathbf{X}$ or $\mathbf{Y}$, the moving window average of the SSIM is evaluated, referred to as the mean SSIM (MSSIM).

$$\mathrm{MSSIM}(\mathbf{X}, \mathbf{Y}) = \frac{1}{M} \sum_{j=1}^{M} \mathrm{SSIM}(\mathbf{x}_j, \mathbf{y}_j) \tag{8}$$

The metric was utilized with its implementation using the package *scikit-image* [33]. We evaluated the MSSIM between the phase reconstructions of the ground truth and the MEF methods. As seen in Fig. 3, our method consistently shows higher MSSIM values for all values of ρ, whereas the improvement in the conventional case remains stagnant even for ρ corresponding to strongly scattering ($\rho = 1.0$) data. Supplement 1 Fig. S2 compares the ptychographic reconstruction results for ρ varying from 0.3 to 1.0 and, as expected, shows improved reconstructions for all cases.

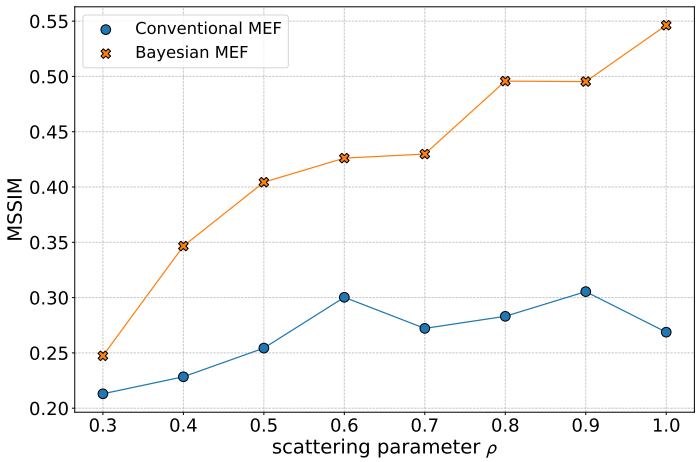

Fig. 3. Evaluating the mean structural similarity index (MSSIM) for reconstructed phase with data generated by varying ρ and fused with the MEF methods.

4. High SNR experimental data with heuristic flux factors

The tests with synthetic data utilized the known flux factors c_i. However, these may or may not be known from an experiment. In the following experimental tests, we have a high SNR and high photon count setting; however, the flux factors are only heuristically known. We demonstrate that the fusion results from the conventional case become unreliable when the flux factors deviate significantly from the actual values. One such case is when the illumination intensity also varies with camera exposure time. In this case, we only have access to heuristic estimate c_i^{heu}. It can be calculated by summing the uncensored data for every acquisition and dividing it by the sum of uncensored data for a fixed acquisition. For example, out of K acquisitions, the fixed acquisition could be the middle one $i = K/2$. The Bayesian MEF approach, outlined in algorithm 1, should iteratively correct the heuristic flux factors by setting $c_i^{(0)} = c_i^{heu.}$. To test this, we constructed a conventional ptychography setup in transmission geometry. A coherent laser source from SuperK COMPACT, offering manual adjustment of the laser power in percentage was employed. We chose a wavelength of 625 nm, a probe size of 400 μm, and used an unstained histological

Optics EXPRESS

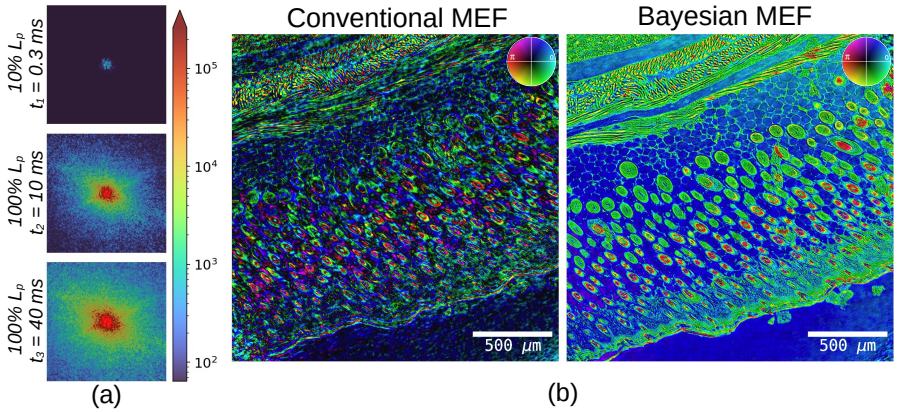

Fig. 4. (a) Diffraction patterns recorded with varying laser power L_p in percentage and camera acquisition times t_i. The second and the third acquisitions are overexposed. (b) Ptychographic reconstructions using the two MEF methods.

mouse section as our test object. Diffraction data was recorded at 500 scan positions using a Lucid CMOS camera with a 12 bit analog-to-digital converter (ADC) and a binning factor of 8, allowing a maximum of 2^{18} counts.

For additional experimental details, please refer to Supplement 1 section 5. We recorded three acquisitions by varying the exposure time and the laser power in percentage (refer to Fig. 4(a)). Each acquisition was repeated thrice, necessitating the fusion of nine diffraction patterns per scan. For each acquisition, 150 dark-frame measurements were recorded and averaged. For the conventional MEF case, we applied the background subtraction procedure to the diffraction patterns and estimated the flux factors heuristically. Subsequently, the conventional MEF method was applied, resulting in a largely unsuccessful ptychographic reconstruction, as depicted in the left panel of Fig. 4(b). However, our method corrects the heuristic flux factors and estimates fused patterns, leading to a high-quality ptychographic reconstruction (see Fig. 4(b), right panel).

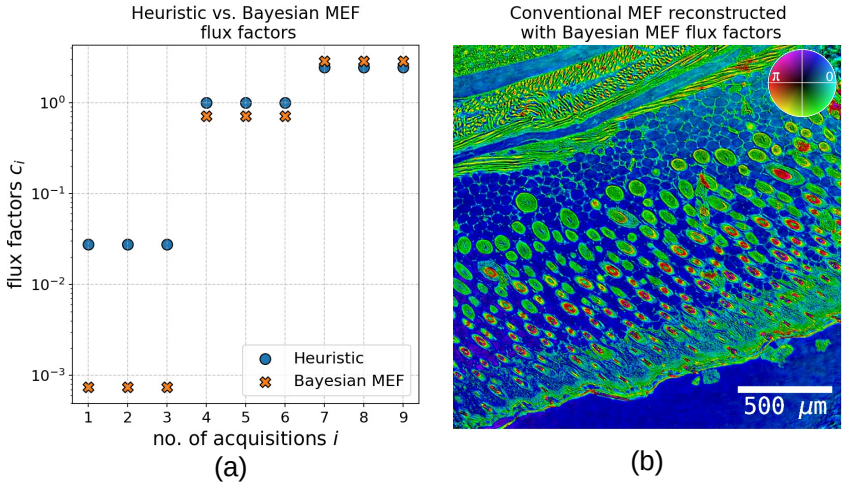

Fig. 5. (a) Heuristic and the corrected Bayesian MEF flux factors (shown in log-scale) for the nine measurements (each acquisition repeated thrice) for every scan position. (b) Conventional MEF reconstruction that used the corrected Bayesian MEF flux factors.

Optics EXPRESS

It is expected that both MEF methods yield comparable results in a high SNR and high photon count scenario, where flux factors are accurately known. This was verified by correcting the heuristic flux factors with our Bayesian MEF approach (step 6 in algorithm 1) as shown in Fig. 5(a) and utilizing them for the conventional MEF case, leading to visually indistinguishable reconstructions (see Fig. 5(b)).

5. Summary

We introduced a Bayesian approach for MEF that incorporates image formation statistics with priors in a principled manner for its application in CDI. Our findings illustrate enhanced HDR phase retrieval, particularly in scenarios, characterized by low SNR or variations in illumination intensity. It can also be noted that conventional MEF is merely a special case of the Bayesian MEF approach, which was verified with the experimental data where both methods perform equivalently with known flux factors in a high count, high SNR regime. Currently, MEF is a preprocessing step for ptychography, and a natural extension of our work would involve the integration of our Bayesian model directly into a ptychography framework based on automatic differentiation (AD) [34], potentially further enhancing robustness in HDR ptychographic reconstructions. Furthermore, exploring physics-informed priors could enhance estimation in scenarios with limited data in the low SNR regime or expedite algorithmic convergence.

In summary, the results presented in this study signify noteworthy advancements in the field of computational imaging. Our work holds promise for robust phase retrieval with challenging weakly scattering specimens or when access to high-quality detectors at extreme wavelengths [3,4] is restricted. Moreover, the versatility of our approach renders it applicable to any imaging scheme requiring enhancement of the dynamic range.

Funding. Carl-Zeiss-Stiftung (CZS Stiftungsprofessuren); Deutsche Forschungsgemeinschaft (HA 5918/4-1, 512648189); Helmholtz Association (ZT-I-PF-4-018 AsoftXm); Freistaat Thüringen; European Social Fund Plus (2023 FGR0053); Open Acess Publication Fund of the Thueringer Universitaets- und Landesbibliothek Jena.

Disclosures. The authors declare no conflicts of interest.

Data availability. In addition to the software package available in Ref. [28], the data used in this work is also available in Ref. [35]. To use the data and reproduce the results in this work, please refer to the details in the GitHub repository of the software.

Supplemental document. See Supplement 1 for supporting content.

References

1. A. M. Maiden and J. M. Rodenburg, "An improved ptychographical phase retrieval algorithm for diffractive imaging," Ultramicroscopy **109**(10), 1256–1262 (2009).
2. J. Rodenburg and A. Maiden, *Ptychography* (Springer International Publishing, 2019), pp. 819–904.
3. P. Thibault, M. Dierolf, A. Menzel, *et al.*, "High-resolution scanning x-ray diffraction microscopy," Science **321**(5887), 379–382 (2008).
4. L. Loetgering, S. Witte, and J. Rothhardt, "Advances in laboratory-scale ptychography using high harmonic sources [invited]," Opt. Express **30**(3), 4133–4164 (2022).
5. K. Ma and Z. Wang, "Multi-exposure image fusion: A patch-wise approach," in *2015 IEEE International Conference on Image Processing (ICIP)*, (2015), pp. 1717–1721.
6. X. Zhang, "Benchmarking and comparing multi-exposure image fusion algorithms," Inf. Fusion **74**, 111–131 (2021).
7. F. Xu, J. Liu, Y. Song, *et al.*, "Multi-exposure image fusion techniques: A comprehensive review," Remote Sens. **14**(3), 771 (2022).
8. Z. Yin, H. Su, E. Ker, *et al.*, "Cell-sensitive phase contrast microscopy imaging by multiple exposures," Med. Image Anal. **25**(1), 111–121 (2015).
9. H. Singh, G. Cristobal, G. Bueno, *et al.*, "Multi-exposure microscopic image fusion-based detail enhancement algorithm," Ultramicroscopy **236**, 113499 (2022).
10. J. Liu, C. Liu, C. Zou, *et al.*, "Large dynamic range dark-field imaging based on microscopic images fusion," Opt. Commun. **528**, 128966 (2023).
11. P. D. Baksh, M. Odstrčil, H.-S. Kim, *et al.*, "Wide-field broadband extreme ultraviolet transmission ptychography using a high-harmonic source," Opt. Lett. **41**(7), 1317–1320 (2016).
12. M. Rose, T. Senkbeil, A. R. von Gundlach, *et al.*, "Quantitative ptychographic bio-imaging in the water window," Opt. Express **26**(2), 1237–1254 (2018).

Optics EXPRESS

13. Y. H. Lo, L. Zhao, M. Gallagher-Jones, *et al.*, "In situ coherent diffractive imaging," Nat. Commun. **9**(1), 1826 (2018).
14. M. Dierolf, P. Thibault, A. Menzel, *et al.*, "Ptychographic coherent diffractive imaging of weakly scattering specimens," New J. Phys. **12**(3), 035017 (2010).
15. M. Stockmar, P. Cloetens, I. Zanette, *et al.*, "Near-field ptychography: phase retrieval for inline holography using a structured illumination," Sci. Rep. **3**(1), 1927 (2013).
16. M. Odstrčil, M. Lebugle, M. Guizar-Sicairos, *et al.*, "Towards optimized illumination for high-resolution ptychography," Opt. Express **27**(10), 14981–14997 (2019).
17. W. Eschen, C. Liu, M. Steinert, *et al.*, "Structured illumination ptychography and at-wavelength characterization with an euv diffuser at 13.5 nm wavelength," Opt. Express **32**(3), 3480–3491 (2024).
18. H. Mimura, S. Handa, T. Kimura, *et al.*, "Breaking the 10 nm barrier in hard-x-ray focusing," Nat. Phys. **6**(2), 122–125 (2010).
19. S. Bajt, M. Prasciolu, H. Fleckenstein, *et al.*, "X-ray focusing with efficient high-na multilayer laue lenses," Light: Sci. Appl. **7**(3), 17162 (2017).
20. W. Eschen, L. Loetgering, V. Schuster, *et al.*, "Material-specific high-resolution table-top extreme ultraviolet microscopy," Light: Sci. Appl. **11**(1), 117 (2022).
21. J. Seifert, Y. Shao, R. van Dam, *et al.*, "Maximum-likelihood estimation in ptychography in the presence of poisson–gaussian noise statistics," Opt. Lett. **48**(22), 6027–6030 (2023).
22. M. Odstrcil, P. Baksh, S. A. Boden, *et al.*, "Ptychographic coherent diffractive imaging with orthogonal probe relaxation," Opt. Express **24**(8), 8360–8369 (2016).
23. S. Shafie, S. Kawahito, I. A. Halin, *et al.*, "Non-linearity in wide dynamic range CMOS image sensors utilizing a partial charge transfer technique," Sensors **9**(12), 9452–9467 (2009).
24. A. P. Dempster, N. M. Laird, and D. B. Rubin, "Maximum likelihood from incomplete data via the em algorithm," J. Royal Stat. Soc. Ser. B (Methodological) **39**(1), 1–22 (1977).
25. P. Thibault and M. Guizar-Sicairos, "Maximum-likelihood refinement for coherent diffractive imaging," New J. Phys. **14**(6), 063004 (2012).
26. A. Gelman, J. B. Carlin, H. S. Stern, *et al.*, *Bayesian Data Analysis* (Chapman and Hall/CRC, 2013).
27. R. L. Plackett, "The truncated poisson distribution," Biometrics **9**(4), 485 (1953).
28. S. Kodgirwar, L. Loetgering, L. Chang, *et al.*, "Supplementary software: Bayesian multi-exposure image fusion for robust high dynamic range ptychography," (2024). https://doi.org/10.5281/zenodo.11103004.
29. M. Treacy and D. Van Dyck, "A surprise in the first born approximation for electron scattering," Ultramicroscopy **119**, 57–62 (2012).
30. A. Maiden, D. Johnson, and P. Li, "Further improvements to the ptychographical iterative engine," Optica **4**(7), 736–745 (2017).
31. L. Loetgering, M. Du, D. B. Flaes, *et al.*, "Ptylab.m/py/jl: a cross-platform, open-source inverse modeling toolbox for conventional and fourier ptychography," Opt. Express **31**(9), 13763–13797 (2023).
32. Z. Wang, A. Bovik, H. Sheikh, *et al.*, "Image quality assessment: from error visibility to structural similarity," IEEE Trans. on Image Process. **13**(4), 600–612 (2004).
33. S. Van der Walt, J. L. Schönberger, J. Nunez-Iglesias, *et al.*, "scikit-image: image processing in python," PeerJ **2**, e453 (2014).
34. S. Kandel, S. Maddali, M. Allain, *et al.*, "Using automatic differentiation as a general framework for ptychographic reconstruction," Opt. Express **27**(13), 18653–18672 (2019).
35. S. Kodgirwar, L. Loetgering, L. Chang, *et al.*, "Supplementary data: Bayesian multi-exposure image fusion for robust high dynamic range ptychography," (2024). https://doi.org/10.5281/zenodo.10964223.